

IV. DISCUSSION

We must stress two facts: (a) If we suppose that the momentum commutes with the coordinate (i.e., we take $\hbar=0$), then in (23) the last term vanishes. The quantum effect is hence contained in this term. (b) In this method, in calculation of the energy, the integrals are not extended over all space but only on some intervals which are determined by the Hamiltonian of the system (via the variational principle). This agrees with the concept of empirical chemistry that a chemical bond exists, i.e., there are some spaces which are more frequently "visited" by electrons than others. Here, this localization is not *a priori* imposed to the system, but results from the principles of quantum mechanics.

APPENDIX

From the commutation relationship between Q and P , one obtains

$$HQ - QH = (i\hbar/2m)P.$$

If f and g are two arbitrary vectors from L^2 , then we have

$$\langle HQf, g \rangle = \langle QHf, g \rangle - (i\hbar/2m)\langle Pf, g \rangle. \quad (A1)$$

Using the spectral resolution formula, we get

$$\begin{aligned} \langle HQf, g \rangle &= \langle Qf, Hg \rangle = \int_{-\infty}^{+\infty} sd_s \langle Q(s)f, Hg \rangle \\ &= \int_{-\infty}^{+\infty} sd_s \langle HQ(s)f, g \rangle. \end{aligned} \quad (A2)$$

On the other hand, we obtain

$$\begin{aligned} \langle QHf, g \rangle - (i\hbar/2m)\langle Pf, g \rangle \\ = \int_{-\infty}^{+\infty} sd_s \langle [Q(s)H - (i\hbar/2m)P(s)]f, g \rangle. \end{aligned} \quad (A3)$$

Using (3) and (2) in (1), one obtains

$$HQ(s) = Q(s)H - P(s)(i\hbar/2m),$$

which proves the lemma.

¹J. E. Lennard-Jones, *Phil. Mag.* **43**, 581 (1952).

²R. S. Mulliken, *Proc. Nat. Acad. Sci. U. S.* **38**, 160 (1953).

³P.-O. Löwdin, *Phys. Rev.* **97**, 1509 (1955); R. Pauncz, J. de Heer, and P.-O. Löwdin, *J. Chem. Phys.* **36**, 2247 (1962); **36**, 2257 (1962); J. de Heer, *ibid.* **37**, 2080 (1962); R. Pauncz, *ibid.* **37**, 2739 (1962); and many subsequent papers.

⁴M. J. S. Dewar and C. A. Wulfman, *J. Chem. Phys.* **29**, 158 (1958); M. J. S. Dewar and H. N. Schmeising, *Tetrahedron* **5**, 166 (1959); **11**, 96 (1960); M. J. S. Dewar and N. L. Hojvat, *J. Chem. Phys.* **34**, 1232 (1961); *Proc. Roy. Soc. (London)* **A264**, 431 (1961); M. J. S. Dewar and N. L. Sabelli, *J. Phys. Chem.*, **66**, 2310 (1962); and many subsequent papers.

Remeasurement of the $2^2S_{1/2}-2^2P_{3/2}$ Splitting in Atomic Hydrogen[†]

B. L. Cosens* and T. V. Vorburger[‡]

Physics Department, Yale University, New Haven, Connecticut 06520

(Received 27 January 1970)

We have completed a remeasurement of the $2^2S_{1/2}-2^2P_{3/2}$ energy separation in atomic hydrogen, using an atomic beam microwave technique. The final result obtained from measurements on four resonances is 9911.173 ± 0.042 MHz. When this is combined with the recent remeasurement by Robiscoe of the $2^2S_{1/2}-2^2P_{1/2}$ energy separation, we obtain a value for the fine-structure splitting ΔE and the fine-structure constant $\alpha^{-1} = 137.0358(5)$.

I. INTRODUCTION

There has been much work done in recent years to remeasure the Sommerfeld fine-structure constant α . We have completed a series of experiments¹ on the fine structure of atomic hydrogen that has yielded a value for the fine-structure splitting ΔE between the states $2^2P_{1/2}$ and $2^2P_{3/2}$

in the $n=2$ level. From this fine-structure separation, the fine-structure constant can be calculated using a well-established theoretical relationship. This result has been published recently,² and it is the purpose of this paper to discuss in detail the techniques used in the experiments.

The work by Lamb, Retherford, Dayhoff, and Triebwasser³ initially opened this first excited

state of hydrogen to microwave spectroscopy. In a pioneering series of atomic beam experiments, they measured the $2^2S_{1/2} - 2^2P_{1/2}$ energy separation \mathcal{S} - now called the Lamb shift - and the $2^2P_{3/2} - 2^2S_{1/2}$ separation $\Delta E - \mathcal{S}$, each to an uncertainty of about 0.1 MHz, approximately $\frac{1}{1000}$ of the width of the P states (see Fig. 1). Of interest to us is the sum of these two numbers, the total $2P$ splitting ΔE . Based on the results obtained by the Lamb group in deuterium, Cohen and DuMond⁴ calculated a value for the fine-structure constant $\alpha^{-1} = 137.0388(6)$. This value was accepted until recently. Meanwhile, a large discrepancy between theory and experiment was being observed in the ground-state hfs splitting in hydrogen. It was thought that the discrepancy arose from difficulties with the hydrogen hfs theory. Since the formula for the hfs was an expansion in powers of α , Greenberg and Foley⁵ suggested an experimental redetermination of α . In the years since then, a number of experiments have done this.

The work reported in this paper is the completion of a series of experiments that has remeasured the fine structure of hydrogen. The method used is similar to that used in the original Lamb experiments. Earlier in the series, Robiscoe and Cosens¹ measured the Lamb shift in H and D. The present measurement of ΔE and \mathcal{S} in H, when combined with the earlier measurement of \mathcal{S} , yields a value for the fine-structure splitting ΔE and the fine-structure constant α .

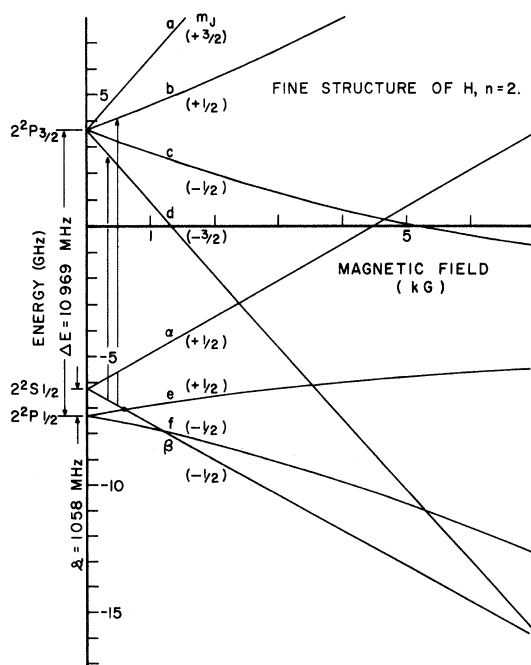


FIG. 1. Zeeman diagram for H, $n=2$. The transitions βb and βd are represented by arrows. The $\beta-e$ crossing is also shown.

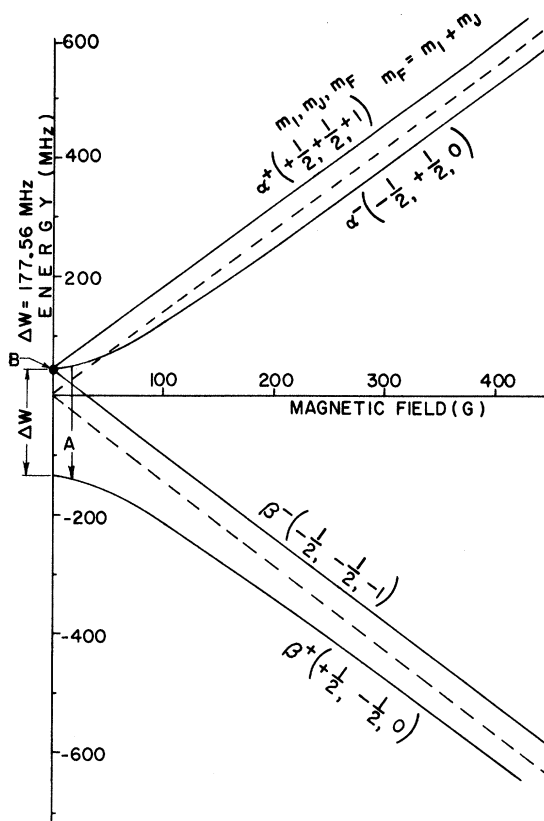


FIG. 2. hfs of the $2^2S_{1/2}$ state. Arrow A represents the rf transition used to populate the β^+ level. Point B represents the Majorana transition used to populate the β^- level. Details of the state selection process are given in LCI and LCII of Ref. 1.

II. EXPERIMENT

A beam of H atoms is produced in the ground state and excited to the $2^2S_{1/2}$ levels α and β by electron bombardment (see Fig. 1). The $2S$ levels are metastable; they live for about $\frac{1}{8}$ sec before decaying to the ground state by two-photon emission. The hfs of the $2S$ state is shown in Fig. 2. At magnetic fields greater than about 100 G, the nuclear angular momentum projection number m_I is a good quantum number. The hyperfine sublevels are labeled α^+ , α^- , β^+ , and β^- , where \pm means $m_I = \pm \frac{1}{2}$. At low magnetic fields, m_I is no longer a good quantum number. m_F is the only projection quantum number used in this representation.

The atoms are quenched in the electron bombardment region (see Fig. 3) by a strong motional field. They are repopulated in a single hyperfine level β^+ or β^- in the state selector (also called the flopper). The beam is then subjected to microwave radiation at a static magnetic field of about 400 G supplied by a Helmholtz coil. The β atoms undergo electric dipole transitions to either the

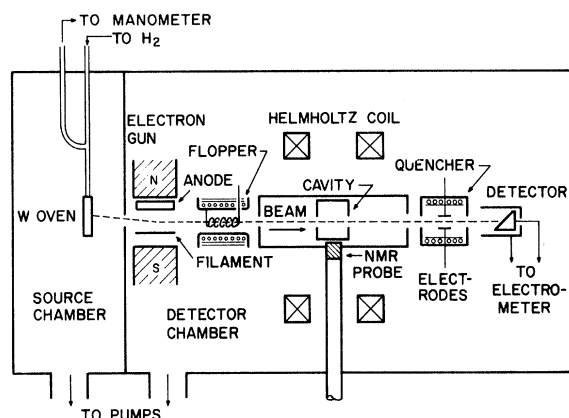


FIG. 3. Schematic diagram of the apparatus.

b or d levels in the $2^2P_{3/2}$ state. The beam then strikes the detector. The rf transitions are observed as a decrease in the metastable population of the beam, as evidenced by a decrease in the detector signal. The frequency of the perturbing electric field is measured to about 1 ppm and the resonance magnetic field is determined to about 150 ppm or about 1 part in 10^3 of the linewidth. An extrapolation to zero magnetic field yields a value of $\Delta E - \delta$ for each transition. We have measured four transitions as shown in Table I.

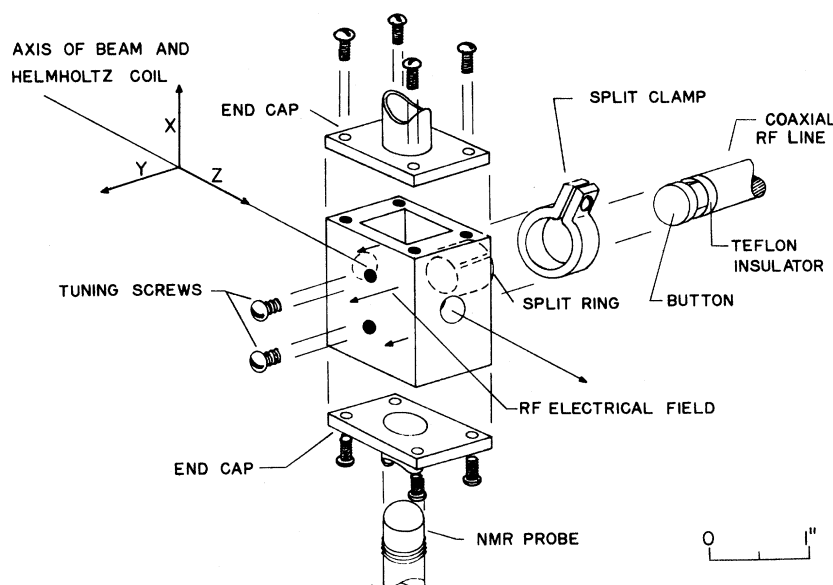
The previous experiments in this series measured the Lamb shift in H and D by inducing dc transitions between the levels β and e . This transition has zero frequency at the $\beta-e$ crossing point near 575 G, as shown in Fig. 1. A precise mea-

TABLE I. Four transitions.

Transition	Initial level	Final level	Approximate frequency (MHz)	Approximate field (G)
βb^-	$m_J = -\frac{1}{2}$ $m_I = -\frac{1}{2}$	$m_J = +\frac{1}{2}$ $m_I = -\frac{1}{2}$	10 845	417
βb^+	$m_J = -\frac{1}{2}$ $m_I = +\frac{1}{2}$	$m_J = +\frac{1}{2}$ $m_I = +\frac{1}{2}$	10 844	375
βd^-	$m_J = -\frac{3}{2}$ $m_I = -\frac{1}{2}$	$m_J = -\frac{1}{2}$ $m_I = -\frac{1}{2}$	9 406	336
βd^+	$m_J = -\frac{3}{2}$ $m_I = +\frac{1}{2}$	$m_J = -\frac{1}{2}$ $m_I = +\frac{1}{2}$	9 406	391

surement of that crossing-point magnetic field yielded the value of δ .

Much of the apparatus has already been described in detail in Ref. 1. Of interest here is the design of the rf system and the quencher. At the center of the Helmholtz coil, the beam enters a rectangular microwave cavity where the electric dipole transitions take place (see Fig. 4). The cavity used for βb transitions has dimensions 1.250 in. high \times 0.480 in. wide \times 0.576 in. long (along the beam axis). It resonates at a frequency of 10 844 MHz. The βd cavity resonates at 9 406 MHz and has dimensions 1.750 \times 0.480 \times 0.659 in. The Q for each cavity is ~ 2000 . The beam passes through $\frac{1}{4}$ -in. holes cut into the front and rear walls. $\frac{3}{8}$ -in. holes are cut into the top and bottom so that a magnetic field probe can be periodically inserted into the center of the transition region. rf power is delivered to the cavity by means of electric coupling. The rf voltage on the button (see Fig. 4) produces an oscillating electric field, which excites the TE_{101} cavity mode. The electric field distribution is perpendicular to the beam and

FIG. 4. Exploded view of the microwave cavity for βb transitions showing the direction of the beam, the magnetic field, and the perturbing electric field.

has the form

$$E_y = E_0 \cos(\pi z/l) \cos(\pi x/h), \quad E_x = E_z = 0, \quad (1)$$

where l is the length of the cavity along the axis and h is the cavity height. Screws are used to tune the cavity frequency by ~ 60 MHz.

The frequency is monitored by a 12-GHz counter and is held constant to ~ 1 ppm by periodic adjustment of the reflector voltage of the klystron. The power level is measured to 1 part in 10^3 by a thin-film thermoelectric power head which generates an emf proportional to the incident power. The klystron delivers about $\frac{3}{4}$ W of rf power, and three attenuators reduce this power to several microwatts entering the cavity. The rf quenching is defined as the difference between the detector signal with the rf switched off and the signal with the rf switched on. $20 \mu\text{W}$ of rf power quenches about 40% of the β state atoms at the center of the βd resonance; for the βb resonance, about $50 \mu\text{W}$ is required.

After the Helmholtz coil, the beam passes through the quencher. This device serves as a switch for the β state component of the beam and is used to eliminate the overlapping α resonances. The quencher consists of a solenoid, which supplies an axial magnetic field of 575 G, and a pair of electrodes, which supply a static electric field of a few volts per centimeter perpendicular to the beam. Iron shielding around the solenoid reduces the stray magnetic field outside the quencher. The use of the quencher is described in Sec. IV.

III. COMPARISON BETWEEN LAMB AND PRESENT EXPERIMENTS

The present experiment induces transitions from a single hyperfine component of the β level. The Lamb experiments worked instead with the α level, which consisted of two hyperfine sublevels. Electric dipole transitions are governed by the selection rule $\Delta m_I = 0$. As a result, the fine-structure transitions were superpositions of two hyperfine resonances. The line shape was consequently broader and more complicated than in the present experiment.

For both experiments the fine-structure levels are split by a magnetic field (see Fig. 1). In the Lamb experiments, this field was oriented perpendicular to the beam. Large motional electric fields, given by $\vec{E} = (\vec{v}/c) \times \vec{H}$, produced appreciable Stark-effect shifts in the energy levels. For example, for the $\alpha-e$ transition, the magnetic field was 1159 G, the motional electric field was 10.6 V/cm , and the Stark shift was 0.46 MHz .⁶ In the present experiment, the magnetic field is oriented parallel to the direction of the beam to reduce these motional fields. Stark shifts are never

greater than 0.023 MHz .

Our use of β state atoms does have some drawbacks, however, since these atoms are easily quenched by motional and stray electric fields. As much as 40% of the β state atoms are quenched near the $\beta-e$ crossing point. This accidental quenching is magnetic field dependent, and it leads to several effects which asymmetrize the resonance lines. These effects will be explained in Sec. VII.

IV. EXPERIMENTAL PROCEDURE

Each run begins with a standard "turn on" procedure. The temperature of the oven is set to $2900 \text{ }^\circ\text{K}$ as measured by an optical pyrometer. The anode voltage of the electron gun is adjusted to produce a maximum number of metastable atoms at the detector. The anode current is held constant at about 1 mA. The state selector or flopper (see Fig. 3) is then adjusted to produce either β^+ or β^- metastable atoms. The field of the Helmholtz coil is set to the approximate center of the β resonance to be studied.

The quencher is adjusted next. With the solenoid set to produce a field of 575 G, the detector signal is measured when the quencher is switched on. This is done as a function of quencher electrode voltage. The resulting quenching curve is shown in Fig. 5. On the plateau of this curve ($V_Q = 3.5 \text{ V}$), essentially all of the β state atoms as well as a few of the α state atoms are quenched. The quenching signal (ΔB_Q) is given by

$$(\Delta B_Q) = N_\beta f_{\beta e} + N_\alpha f_{\alpha f}, \quad (2)$$

where $f_{\beta e}$ and $f_{\alpha f}$ are the fractions of β and α state atoms quenched by the dc electric field (at 3.5 V , $f_{\beta e} \approx 98\%$, and $f_{\alpha f} \approx 2\%$). The β signal is obtained by extrapolating along the quenching plateau to zero voltage. For example, in run 29 (see Fig. 5) N_β is equal to 690 galvanometer divisions. A voltage

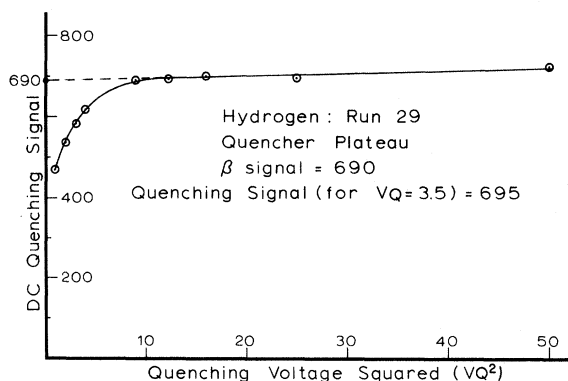


FIG. 5. Quencher plateau for run 29. The dc quenching signal has the units of galvanometer divisions. Extrapolation of the sloping α plateau to 0 V gives the total signal due to atoms in the β state.

of 3.5 V quenches this amount of beam. Therefore,

$$(\Delta B_Q)_{3.5} = N_\beta, \text{ for run 29.} \quad (3)$$

The other parameters in Eq. (2) can be determined using the quencher as well. For $V_Q = 400$ V, more than 99.9% of all the metastable atoms are quenched. Hence, the total metastable population $N_\alpha + N_\beta$ can be determined:

$$(\Delta B_Q)_{400} = N_\alpha + N_\beta. \quad (4)$$

Thus, we have

$$N_\alpha = (\Delta B_Q)_{400} - (\Delta B_Q)_{3.5}. \quad (5)$$

To determine $f_{\alpha f}$, the flopper is temporarily adjusted so that the β state atoms are no longer being produced. Then the ratio $(\Delta B_Q)_{3.5} / (\Delta B_Q)_{400}$ yields $f_{\alpha f}$:

$$(\Delta B_Q)_{3.5} / (\Delta B_Q)_{400} = N_\alpha f_{\alpha f} / N_\alpha. \quad (6)$$

These values can now be substituted into Eq. (2) to yield $f_{\beta e}$. For run 29 these four parameters are

$$N_\beta = 690, \quad N_\alpha = 890, \quad f_{\beta e} = 0.976, \quad f_{\alpha f} = 0.018. \quad (7)$$

For the remainder of the run, the flopper is readjusted to produce β state atoms, and the quencher voltage is reset so that (ΔB_Q) is equal to N_β again. For run 29 this voltage is 3.5 V.

A resonance curve is taken next. The rf power level is adjusted to quench between 20% and 50% of the β state atoms at the center of the resonance. A panoramic view of the resonance is taken. The curve taken in run 23 is shown in Fig. 6. At each field setting, three measurements are taken. First, the rf quenching is measured with the quencher off. This signal, called $(\Delta B_{rt})_{Q \text{ off}}$, is shown in Fig. 6(a) and is given by

$$(\Delta B_{rt})_{Q \text{ off}} = N_\alpha f_\alpha + N_\beta f_\beta. \quad (8)$$

Here f_α and f_β are the fractions of α and β state atoms that are quenched by rf in the Helmholtz coil.

Next the rf quenching is measured with the dc quencher on. This curve is shown in Fig. 6(b). Since very few β state atoms survive transit through the quencher, no rf β resonance is observed. This signal, called $(\Delta B_{rt})_{Q \text{ on}}$, is given by

$$(\Delta B_{rt})_{Q \text{ on}} = N_\beta(1 - f_{\beta e})f_\beta + N_\alpha(1 - f_{\alpha f})f_\alpha. \quad (9)$$

Curve b is subtracted point by point from curve a to yield the almost pure rf β quenching signal.

The quenching fraction F is defined as this signal divided by the total β signal $(\Delta B_Q)_{3.5}$. It is given by

$$F = \frac{(\Delta B_{rt})_{Q \text{ off}} - (\Delta B_{rt})_{Q \text{ on}}}{(\Delta B_Q)_{3.5}}$$

$$= \frac{f_\beta + (N_\alpha/N_\beta)(f_{\alpha f}/f_{\beta e})f_\alpha}{1 + (N_\alpha/N_\beta)(f_{\alpha f}/f_{\beta e})}. \quad (10)$$

This expression is a synthetic fractional quenching which consists of two parts: (a) the rf fractional β quenching and (b) the rf fractional α quenching reduced by about a factor of 20. If the dc αf quenching were equal to zero, the α overlap would disappear completely.⁷ The small asymmetry due to the remaining overlapping α resonance is discussed later.

Finally, a series of center measurements is taken. Two magnetic field values, the upper and lower working points, are selected at which the rf quenching is about 75% of the central field quenching. The slope of the quenching resonance is a maximum at these points, and a comparison of the values of F at these points yields a sensitive determination of the central magnetic field H_c :

$$H_c = (F_+ - F_-) / 2(dF/dH)_{av} + \frac{1}{2}(H_+ + H_-). \quad (11)$$

F_+ and F_- are the values for the fractional quenching at the upper and lower working points, respectively, and $(dF/dH)_{av}$ is the average value of the magnitude of the experimentally determined slope at the working points. A typical run includes between 10 and 20 measures of the center.

While the center measurements are being taken,

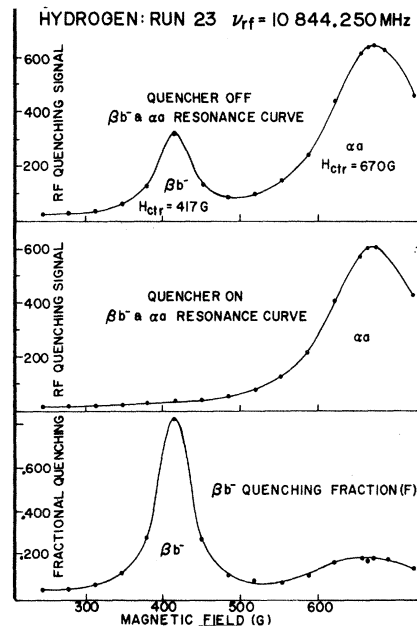


FIG. 6. rf resonances for run 23. (a) With quencher off: Graph shows $\beta\beta^-$ and overlapping $\alpha\alpha$. (b) With quencher on: The β state atoms are quenched. Graph shows only $\alpha\alpha$ resonance. (c) rf quenching fraction F given by the difference between (a) and (b) divided by the total β signal.

the NMR probe is inserted periodically into the transition region, and the magnetic field is measured at the upper and lower working points. A good run yields a value for the central magnetic field precise to about 150 ppm or about one part per thousand of the linewidth.

V. DATA

The graph of fractional quenching is shown in Fig. 6(c). Since the quantities $f_{\alpha f}$, $f_{\beta e}$, N_{α} , and N_{β} have been measured, f_{α} can be determined from Fig. 6(b); and F can be corrected for the α overlap to yield the fractional quenching f_{β} . A line shape corrected for α overlap in this manner is shown as a series of data points in Fig. 7. The line shown is the theoretical curve derived using the Bethe-Lamb theory for the lifetime of the metastable state under an external perturbation.⁸ This line shape theory can be tested by comparison with the experimentally observed half-widths. The ratios of the experimental half-width to the theoretical half-width ($\delta H_E / \delta H_T$) averaged over all the runs for each transition are

$$\left(\frac{\delta H_E}{\delta H_T}\right)_{\beta d} = 0.992 \pm 0.009, \quad \left(\frac{\delta H_E}{\delta H_T}\right)_{\beta d} = 0.999 \pm 0.008. \quad (12)$$

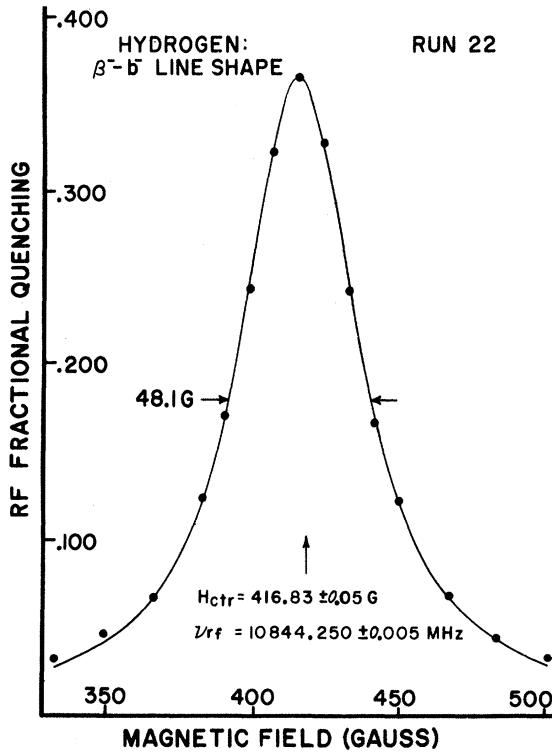


FIG. 7. Quenching fraction f_{β} for run 22. The experimental points are corrected for α overlap. The theoretical curve is derived using the Bethe-Lamb theory for the lifetime of the $2S$ state under a perturbing electric field. The line shape is averaged over a v^4 velocity distribution.

The main pieces of data used to determine the center of the resonance are measures of the fractional quenching F at each working point, measures of the nuclear magnetic resonance (NMR) frequency at each working point, and the average magnitude of the line slope at the working points. The NMR measurements themselves yield a value for the nominal center $(\nu_0)_{\text{NMR}}$ given by

$$(\nu_0)_{\text{NMR}} = \frac{1}{2}(\nu_+ + \nu_-)_{\text{NMR}}. \quad (13)$$

These working points are selected to be as close as is convenient to the three quarter points on the resonance curve. However, to correct for small deviations, the actual working points are extrapolated along the slopes of the resonance curve to equalized quenching points. This gives a correction to the central NMR frequency $(\delta\nu)_{\text{NMR}}$

$$(\delta\nu)_{\text{NMR}} = (F_+ - F_-)/2(dF/d\nu)_{\text{av}}, \quad (14)$$

where $(dF/d\nu)_{\text{av}}$ is the average magnitude of the slope of the resonance curve at the working points. Thus, the observed center of the resonance curve is taken to be

$$(\nu_{\text{ctr}})_{\text{NMR}} = (\nu_0)_{\text{NMR}} + (\delta\nu)_{\text{NMR}}. \quad (15)$$

Typical numbers for one run are as follows (run 22 - a βb^- run in this example): $(\nu_0)_{\text{NMR}} = 1774.555 \pm 0.103$ kHz, $[\frac{1}{2}(F_+ - F_-)]_{\text{av}} = (+3.43 \pm 5.03) \times 10^{-4}$, $(dF/d\nu)_{\text{av}} = 2.580 \times 10^{-3}$ /kHz, $(\delta\nu)_{\text{NMR}} = +0.133 \pm 0.195$ kHz, $(\nu_{\text{ctr}})_{\text{NMR}} = 1774.688 \pm 0.220$ kHz. The errors quoted are, in each case, one standard deviation of the mean.

The magnetic field variable ($\mu_B H$) is related to the proton NMR frequency ν_{NMR} in water by

$$\nu_{\text{NMR}} = g_p(\text{H}_2\text{O})\mu_B H, \quad (16)$$

where μ_B is the Bohr magneton. $g_p(\text{H}_2\text{O})$, the proton g factor in water, can be written in terms of the free-electron g factor g_S and the bound-electron g factor in the ground state of hydrogen, $g_J(\text{H})$:

$$g_p(\text{H}_2\text{O}) = g_S \frac{g_J(\text{H})/g_S}{g_J(\text{H})/g_p(\text{H}_2\text{O})}. \quad (17)$$

The quantities on the right-hand side of Eq. (17) are all known. The value of g_S is $2.002319114(60)$.⁹ In addition, we have the relativistic correction¹⁰

$$g_J(\text{H})/g_S = 1 - \frac{1}{3}\alpha^2, \quad (18)$$

and the value for $g_J(\text{H})/g_p(\text{H}_2\text{O})$ measured by Lambe¹¹ is

$$g_J(\text{H})/g_p(\text{H}_2\text{O}) = 658.21591(4). \quad (19)$$

The resulting formula for $\mu_B H$ is

$$\begin{aligned} \mu_B H &= \frac{g_J(\text{H})/g_p(\text{H}_2\text{O})}{g_S(1 - \frac{1}{3}\alpha^2)} \nu_{\text{NMR}} \\ &= 328.73261(2) \nu_{\text{NMR}}. \end{aligned} \quad (20)$$

VI. ANALYSIS

Two different approaches to the Hamiltonian for the S and P states are used to analyze the data.

The first approach is a perturbation treatment of Lamb's Hamiltonian for H, $n=2$, contained in HIII.³ The matrix elements are calculated in the $\vec{J}, \vec{I}, m_J, m_I$ representation. This is the most realistic representation for a magnetic field of 400 G. \vec{L} and \vec{S} are strongly coupled to \vec{J} ; \vec{I} and \vec{J} are decoupled.

The second approach is a computer diagonalization of Brodsky and Parsons's¹² (BP) Hamiltonian for H, $n=2$. Brodsky and Parsons state that their analysis of the Zeeman structure is intrinsically accurate to 0.001 MHz. The BP Hamiltonian is calculated in the low-field representation: $\vec{J}, \vec{I}, \vec{F}$, and m_F . It includes some corrections due to radiative and nuclear motion effects and is, therefore, more accurate than the Lamb Hamiltonian. Consequently, our final results are based on the BP Hamiltonian. Use of the Lamb Hamiltonian gives results which never differ by more than 0.018 MHz or 2 ppm in $\Delta E - s$ from those obtained with the BP Hamiltonian. Most of this discrepancy arises because the Lamb treatment expresses the hyperfine splitting of the $2P$ states in terms of the splitting of the $2S$ state ΔW ($=177.55686(5)$ MHz).¹³ BP express the hyperfine splitting in terms of the Fermi energy $E_F(H)$, which is related to ΔW by¹⁴

$$E_F(H) = (2/g_s) \Delta W [1 + O(\alpha^2)]. \quad (21)$$

The factor $(2/g_s)$ introduces discrepancies in the P state energies of the order of 0.01 MHz.¹⁵

VII. CORRECTIONS TO THE DATA

Before the observed resonance centers and rf frequencies can be analyzed to yield values for

$\Delta E - s$, a number of corrections need to be applied. Several effects asymmetrize the resonances we study, and shift the apparent center from the true center. Average values of the corrections for each transition are listed in Table II together with an estimate of their 68% confidence intervals.

A. Variation of the rf Matrix Element

The transition probability is proportional to $|\langle S | e \vec{E} \cdot \vec{r} | P \rangle|^2$. For βb^- transitions, this matrix element decreases with magnetic field due to $\vec{L} \cdot \vec{S}$ decoupling of the states b and e . Consequently, the high-field side of the resonance curve appears lower than the low-field side, and the apparent center is below the true center. For βb^+ and βd^+ transitions, the matrix element increases with magnetic field due to $\vec{I} \cdot \vec{J}$ decoupling of the states β^+ and α^- . The apparent center is thereby shifted upward.

B. Level Curvature

The $\vec{L} \cdot \vec{S}$ and $\vec{I} \cdot \vec{J}$ interactions in the Hamiltonian produce curvature of the Zeeman lines. Consequently, the energy level separation is asymmetric about the center of the resonance.

C. Finite Size of the rf Region

The cavity produces an rf electric field which extends over about 0.6 in. of beam path length. The mean rf quenching then occurs at a magnetic field lower than the measured central field, and this mean quenching becomes resonant when the measured central field is higher than the resonant field. The resonance center thereby appears above the true center.

TABLE II. Average values of the asymmetry corrections (MHz).

Transition corrections	βb^-	βb^+	βd^-	βd^+
rf matrix element variation	-0.105 ± 0.010	-0.096 ± 0.013		-0.042 ± 0.006
Level curvature	-0.006 ± 0.001	-0.019 ± 0.002		-0.026 ± 0.003
Finite extent of the rf region	$+0.019 \pm 0.002$	$+0.018 \pm 0.002$	-0.019 ± 0.002	-0.022 ± 0.002
αc overlap			$+0.028 \pm 0.021$	$+0.010 \pm 0.008$
αa overlap	$+0.049 \pm 0.053$	$+0.032 \pm 0.028$	$+0.001$	$+0.002$
β population variation	-0.009 ± 0.001	$+0.004$	-0.001	$+0.029 \pm 0.003$
Velocity distribution distortion	-0.013 ± 0.004	-0.018 ± 0.007	$+0.002 \pm 0.001$	$+0.042 \pm 0.012$
βd overlap	-0.009	-0.006		
βb overlap			$+0.003$	$+0.003$
βc and αb overlap	$+0.001 \pm 0.001$	0.000 ± 0.001	0.000 ± 0.001	0.000 ± 0.001
Forbidden transitions	0.000	0.000 ± 0.002	0.000 ± 0.001	0.000
rf Stark shift	-0.006	-0.005	-0.003	-0.004
dc Stark shift	$+0.023 \pm 0.005$	$+0.020 \pm 0.004$	$+0.005 \pm 0.001$	$+0.017 \pm 0.003$
β^- impurities	0.000	0.000 ± 0.021	0.000	0.000 ± 0.050
Hamiltonian and roundoff	0.000 ± 0.006	0.000 ± 0.006	0.000 ± 0.006	0.000 ± 0.006
Sum	-0.057 ± 0.055	-0.070 ± 0.039	$+0.016 \pm 0.022$	$+0.009 \pm 0.053$

D. Overlapping Resonances

The αc overlap on the βd transitions and the αa overlap on the βb transitions have already been described (see Fig. 6). The calculation of these corrections is performed in two ways. First, one can calculate the overlap directly from the known parameters of the α resonance. When the size of the direct overlap is reduced by the factor $(N_\alpha/N_\beta)(f_{\alpha f}/f_{\beta a})$ [see Eq. (10)] because of the use of the quencher, a fractional shift in the center of the β resonance is obtained. For example, for run 21, this is a fractional shift of center $(\delta H/H_{ctr}) = -11$ ppm. The alternative method is to sweep the magnetic field through the overlapping α resonance and observe the height of F at the center of the α resonance. In all cases, the amount of observed α resonance present is larger than expected. For example, for run 21 again, the correction to the observed center obtained by this method is $(\delta H/H_{ctr}) = -60$ ppm. There is a discrepancy of 49 ppm between these two methods. Since the quencher is located very close to the detector, this discrepancy may arise from a change in the detector efficiency when the quencher is turned on. In all cases, we have evaluated the correction by taking the average value obtained by the two methods. So for run 21, this would be $-(36 \pm 29)$ ppm. The error is taken to enclose the results of both methods.

E. Population Variation

The metastable beam diverges slightly as it traverses the machine. In addition, it may be tilted slightly with respect to the Helmholtz coil axis. Motional electric fields result from both of these effects. Stray charges may build up inside the cavity due to oil condensation on the surfaces. Both the motional and stray electric fields cause static quenching of the beam. Since these effects are magnetic field dependent, there is a variation of the β population with magnetic field.

F. Velocity Distribution Distortion

The beam is assumed to have a normalized Maxwellian v^4 velocity distribution. Motional electric fields preferentially quench fast atoms while the stray static fields preferentially quench slow atoms. There is a resulting velocity distribution distortion which is magnetic field dependent and which asymmetrizes the line shape. The correction for this was first calculated by Robiscoe¹⁶ for the crossing-point experiments. This earlier calculation was made assuming a v^2 velocity distribution. However, Robiscoe and Shyn¹⁷ have recently measured the velocity distribution on an apparatus very similar to the apparatus used in our

experiments. They find that a recoil effect in the electron gun tends to knock slower metastable atoms out of the beam. This produces the change from a v^2 to a v^4 character for the velocity distribution.

This discovery caused a change of 0.04 MHz in the value of the Lamb shift as determined from the crossing-point experiments. These present experiments are not as sensitive to this effect, however, since the two fine-structure transitions βb and βd have opposite field dependences and thereby tend to cancel out errors in these distortion calculations.

G. Overlapping σ Transitions

Components of the electric field parallel to the magnetic field will induce βc and αb transitions. We estimate an upper limit on any such electric fields to be 10% of the main quenching field. We add corrections due to these overlapping resonances into the error calculations in Table II.

H. Forbidden Transitions

The level d^+ is mixed with c^- by the $\vec{I} \cdot \vec{J}$ interaction in the Hamiltonian. The c^- level is coupled to β^- by the $\vec{E}_\parallel \cdot \vec{r}$ matrix element. Thus, there is a possibility of inducing the forbidden $\beta^- d^+$ transition which overlaps the $\beta^- d^-$ transition. The ratio R of the strength of the $\beta^- d^+$ transition to the strength of the $\beta^- d^-$ is¹⁸

$$R = \left(\frac{\Delta W}{15g_J\mu_B H} \right)^2 \frac{|\langle c^- | \vec{I} \cdot \vec{J} | d^+ \rangle|^2}{|\langle \beta^- | \vec{E}_\parallel \cdot \vec{r} | c^- \rangle|^2} \frac{|\langle \beta^- | \vec{E}_\parallel \cdot \vec{r} | d^+ \rangle|^2}{|\langle \beta^- | \vec{E}_\parallel \cdot \vec{r} | d^- \rangle|^2}. \quad (22)$$

Similarly, it is possible to induce the $\beta^+ b^-$ transition which overlaps $\beta^+ b^+$. The 10% upper limit for E_\parallel used before yields contributions to the error as shown in Table II.

J. dc Stark Shifts

The small motional and stray dc electric fields couple the β state to the nearby e state and produce a shift in the β energy.

K. rf Power Shift

There is a shift in the separation of the initial and final states of the rf transition due to state mixing by the antiresonant component of the perturbing electric field. Lamb has given a complete discussion of this shift in VIII, Appendix D.

L. Beam Impurities

We estimate an upper limit of 1 part in 350 on the contamination of a β^+ state beam by β^- atoms produced by a Majorana transition in the flopper. The correction resulting from this contamination is added to the error estimate of the βb^+ and βd^+ transitions.

M. Hamiltonian and Roundoff Errors

We estimate the roundoff error to be ± 0.006 MHz. The Brodsky-Parsons Hamiltonian has a quoted accuracy of 0.001 MHz.

VIII. RESULTS

The results for each run are listed in Table III. The corrections are added to each run. Uncertainty in the corrections is not included in the uncertainty for an individual run. It is felt that these are more characteristic of the transition and that their effects would be masked by quadratically adding them to the large statistical error of each run. An uncertainty of one standard deviation of the mean (σ) is calculated from the scatter in the data for each run. An average value of $\Delta E - \delta$ is found for each transition by weighting each run as $1/\sigma^2$. These results are shown in Table IV. The final error for each transition is found by taking a quadratic sum of the statistical uncertainty and the systematic uncertainty given in Table II.

The final value for $\Delta E - \delta$ is the weighted average of the four transition values

$$\Delta E - \delta = 9911.173 \pm 0.042 \text{ MHz.} \quad (23)$$

The quoted uncertainty is one standard deviation of the mean of the four values. The variance of the four values about the mean is 0.040 MHz.

In order to calculate ΔE we add the experimental value for the Lamb shift obtained by Robiscoe on the same apparatus and recently corrected for the v^4 beam velocity distribution distortion.¹⁷ This result is $\delta = 1057.896 \pm 0.063$ MHz.¹⁹ ΔE is then given by

$$\Delta E = (\Delta E - \delta) + \delta = 10969.069 \pm 0.076 \text{ MHz.} \quad (24)$$

We use the formula for ΔE discussed by Taylor, Parker, and Langenberg²⁰ to derive a value for α^{-1} :

$$\alpha^{-1} = 137.0358(5). \quad (25)$$

TABLE III. Summary of runs.

Transition	Run	Numbers of centers	Run correction (MHz)	$\Delta E - \delta$ (MHz)	Statistical error (σ) (MHz)	Weight
βb^-	10	7	-0.028	9910.966	0.521	0.021
	11	7	-0.065	9911.275	0.176	0.182
	12	20	-0.097	9911.104	0.248	0.091
	14	20	-0.040	9911.324	0.130	0.331
	22	10	-0.054	9911.307	0.122	0.375
βb^+	17	11	-0.053	9911.072	0.145	0.273
	19	20	-0.073	9910.911	0.180	0.176
	20	20	-0.085	9911.262	0.115	0.428
	21	20	-0.076	9911.224	0.216	0.123
βd^-	27	18	0.028	9911.239	0.186	0.153
	28	25	0.004	9911.188	0.079	0.847
βd^+	29	6	0.012	9911.082	0.096	0.463
	30	20	0.011	9910.988	0.149	0.192
	31	20	0.005	9911.140	0.111	0.345

TABLE IV. Final results.

Transition	$\Delta E - \delta$ (MHz)	Statistical error (MHz)	Systematic error from Table II (MHz)	Total error (MHz)	Weight
βb^-	9911.281	0.074	0.055	0.092	0.207
βb^+	9911.144	0.076	0.039	0.085	0.241
βd^-	9911.196	0.073	0.022	0.076	0.302
βd^+	9911.084	0.065	0.053	0.084	0.250
Final result: $\Delta E - \delta = 9911.173 \pm 0.042$ MHz					

IX. DISCUSSION

Our result for $\Delta E - \delta$ may be compared with the results of Shyn, Williams, Robiscoe, and Rebane²¹ and with the results of Kaufman, Lamb, Lea, and Leventhal.²²

The apparatus of Shyn *et al.* is similar to ours. They have measured βb^+ and βd^+ transitions at magnetic fields of ~ 850 G. For each transition their results are

$$\begin{aligned} (\Delta E - \delta)_{\beta b^+} &= 9911.255 \pm 0.059 \text{ MHz,} \\ (\Delta E - \delta)_{\beta d^+} &= 9911.242 \pm 0.090 \text{ MHz,} \end{aligned} \quad (26)$$

and their final average from 115 line centers is 9911.250 ± 0.063 MHz. The difference between their result and ours is 0.077 ± 0.076 MHz.

Kaufman *et al.* made a determination of $\Delta E - \delta$ in H, $n = 2$, by measuring αa and αb transitions at ~ 1600 G. They did not use an atomic beam method. Instead, the entire process of dissociation, excitation, and rf transition took place inside a small interaction region. The signal depended on the emission of the Lyman- α radiation. Their result was $\Delta E - \delta = 9911.38 \pm 0.03$ MHz. This disagrees with the present result by 0.22 ± 0.05 MHz or about four standard deviations.

There has been one other recent experiment on H fine structure. Metcalf, Brandenberger, and Baird²³ made a redetermination of ΔE by measuring the $e-d$ level crossing shown in Fig. 1. In their experiment, Lyman- α radiation was scattered by H atoms in the 2^2P state. The angular distribution of this radiation changed near the crossing of these two levels. Their result was $\Delta E = 10969.13 \pm 0.12$ MHz, and $\alpha^{-1} = 137.0354(7)$.

All of these fine-structure experiments have relied on the ability to split the resonance line to about one part in a thousand of its width. Consequently, systematic corrections have been extremely critical.

These recent results for α from H fs measurements may be compared with other precision experiments. There has been some controversy over the years. The experiments are summarized below, and the results are shown in Fig. 8.²⁴

(a) The experiments of Lamb *et al.* on the fine

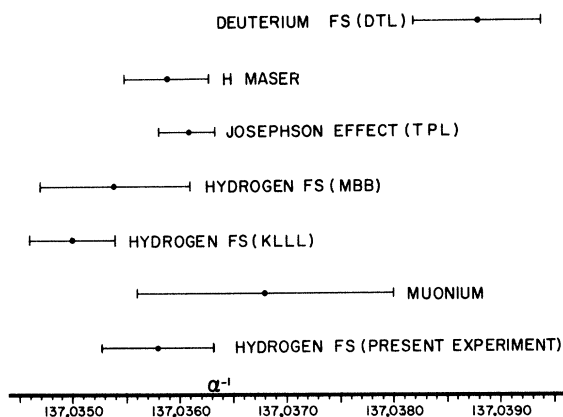


FIG. 8. Fine-structure constant α determined from seven experiments including the present one.

structure of deuterium provided the determination of $\alpha^{-1} = 137.0388(6)$.

(b) Experiments utilizing a hydrogen maser²⁵ provided a measurement of the hfs splitting in the ground state of hydrogen. The results, when combined with the theoretical calculations,²⁶ have yielded a value for α^{-1} ,²⁷ which is smaller than the Lamb value by 21 ppm: $\alpha^{-1} = 137.0359(4)$.

(c) Measurements of the hfs interval in the ground state of muonium²⁸ at first confirmed the result of Lamb. However, a shielding correction to the magnetic moment of the muon, suggested by Ruderman,²⁹ and a recent remeasurement of the hfs interval at low magnetic fields by Thompson *et al.*³⁰ has shifted the value of α^{-1} to 137.0368(11).

(d) Experiments by Parker, Taylor, and Langenberg¹⁹ utilizing the ac Josephson effect in superconductors have measured e/h to a high accuracy. Their number yields a value for α^{-1} : $\alpha^{-1} = 137.03608(26)$. This is the most precise experimental determination of the constant to date, and it agrees with the result from H hfs.

The experiments on H fine structure reveal a

fair amount of disagreement (see Fig. 8). Our own result agrees with that of Metcalf *et al.* and confirms the e/h experiment. It disagrees with the original Lamb experiments and with Kaufman *et al.*

A simple weighted average of the four H and D fs values for α^{-1} yields $\alpha^{-1} = 137.0360(8)$. The error quoted is the variance of the four values. It is large, because the original Lamb measurement disagrees with the others by ~ 20 ppm.

Taylor, Parker, and Langenberg¹⁹ have published a readjustment of the fundamental constants in the light of these recent experiments. They have chosen only to include the H hfs work and their own e/h work in the readjustment for α . They feel that the accuracy in the published work of Kaufman *et al.* and Metcalf *et al.* may have been overestimated, and that the disagreement between the experimental^{1,3} and the theoretical³¹ values of \mathcal{S} casts some degree of doubt on both. If the experimental uncertainties are expanded to encompass these difficulties, the H fine-structure experiments would carry negligible weight in the adjustment for α . However, Appelquist and Brodsky³² have recently discovered a correction to the theoretical value for \mathcal{S} , which places it in agreement with the experimental value. This new development may change the status of the H fine structure experiments in the readjustment for α .

Possibilities exist for another determination of α . Pichanick, Swift, Johnson, and Hughes³³ have measured the $2^3P_1 - 2^3P_2$ fine structure in helium to a precision of 3 ppm.³⁴

In general, we feel that these experiments on the fine structure of hydrogen can serve, at best, as confirming the more accurate methods of measuring the fine-structure constant.

ACKNOWLEDGMENTS

The support and encouragement of Professor William Lichten is gratefully acknowledged. Our thanks also go to R. Reno and Dr. S. Kaufman for many valuable discussions.

[†]Work supported by the National Science Foundation.

*Present address: St. Olaf College, Northfield, Minn. 55057.

[‡]Present address: Physics Dept., University of Delaware, Newark, Del. 19711.

¹The following papers will be referred to as LCI-LCIV: LCI, R. T. Robiscoe, *Phys. Rev.* **138**, A22 (1965); LCII, R. T. Robiscoe and B. L. Cosens, *Phys. Rev. Letters* **17**, 69 (1966); LCIII, B. L. Cosens, *Phys. Rev.* **173**, 49 (1968); and LCIV, B. L. Cosens and T. V. Vorburger, *Phys. Rev. Letters* **23**, 1273 (1969).

²LCIV, Ref. 1.

³This series of six papers will be referred to as HI-HVI: HI, W. E. Lamb, Jr., and R. C. Retherford, *Phys. Rev.* **79**, 549 (1950); HII, W. E. Lamb, Jr. and R. C. Retherford, *ibid.* **81**, 222 (1951); HIII, W. E. Lamb, Jr., *ibid.* **85**, 259 (1952); HIV, W. E. Lamb, Jr., and R. C. Retherford, *ibid.* **86**, 1014 (1952); HV, S. Triebwasser, E. S. Dayhoff, and W. E. Lamb, Jr., *ibid.* **89**, 98 (1953); HVI, E. S. Dayhoff, S. Triebwasser, and W. E. Lamb, Jr., *ibid.* **89**, 106 (1953).

⁴E. R. Cohen and J. W. M. DuMond, *Rev. Mod. Phys.*

37, 537 (1965).

⁵D. A. Greenberg and H. M. Foley, *Phys. Rev.* 120, 1684 (1960).

⁶These numbers were taken from HIII, Ref. 3, p. 267.

⁷The alternative method for reducing the overlapping α resonances is to go to higher magnetic fields. This inherently simpler method would have required the construction of an entire new high-field Helmholtz coil.

⁸HI, Appendix B, and HIII, Appendix D of Ref. 3. See also H. A. Bethe and E. E. Salpeter, *Quantum Mechanics of One and Two Electron Atoms* (Academic, New York, 1957), Sec. 67.

⁹D. T. Wilkinson and H. R. Crane, *Phys. Rev.* 130, 852 (1963). Their result has been corrected by A. R ch, *Phys. Rev. Letters* 20, 967 (1968).

¹⁰For a good discussion of g factors, see T. Myint, D. Kleppner, N. F. Ramsey, and H. G. Robinson, *Phys. Rev. Letters* 17, 405 (1966).

¹¹E. B. D. Lambe, thesis, Princeton University, 1959 (unpublished).

¹²S. J. Brodsky and R. G. Parsons, *Phys. Rev.* 163, 134 (1967).

¹³J. W. Heberle, H. A. Reich, and P. Kusch, *Phys. Rev.* 101, 612 (1956).

¹⁴See in Ref. 12, Ref. 11.

¹⁵This factor was mentioned by Lamb in HIII, Ref. 3, Appendix VI (c). However, their experiments were insensitive to this discrepancy since the transitions observed were hyperfine doublets.

¹⁶R. T. Robiscoe, *Phys. Rev.* 168, 4 (1968).

¹⁷R. T. Robiscoe and T. W. Shyn (private communication).

¹⁸Another discussion of the forbidden transitions is given in HIV, Ref. 3, Sec. 74.

¹⁹Their result appears on p. 488 of B. N. Taylor, W. H. Parker, and D. N. Langenberg, *Rev. Mod. Phys.* 41, 375 (1969).

²⁰Reference 19, p. 461.

²¹T. W. Shyn, W. L. Williams, R. T. Robiscoe, and T. Rebane, *Phys. Rev. Letters* 22, 1273 (1969), and (private communication).

²²S. L. Kaufman, W. E. Lamb, Jr., K. R. Lea, and M. Leventhal, *Phys. Rev. Letters* 22, 507 (1969).

²³H. Metcalf, J. R. Brandenberger, and J. C. Baird, *Phys. Rev. Letters* 21, 165 (1968); J. R. Brandenberger, thesis, Brown University, 1968 (unpublished). The thesis contains the latest result of $\alpha^{-1}=137.0354(7)$.

²⁴We have not included a value for α derived from the measurement of $\Delta E - S$ by Shyn *et al.* This group is currently remeasuring the Lamb shift which will be combined with $\Delta E - S$ to yield ΔE and α .

²⁵S. B. Crampton, D. Kleppner, and N. F. Ramsey, *Phys. Rev. Letters* 11, 338 (1963); R. Vessor *et al.*, *IEEE Trans. Instr. Meas.* IM-15, 165 (1966).

²⁶S. J. Brodsky and G. W. Erickson, *Phys. Rev.* 148, 26 (1966); S. D. Drell and J. D. Sullivan, *ibid.* 154, 1477 (1967).

²⁷See Ref. 19, p. 449.

²⁸W. E. Cleland, J. M. Bailey, M. Eckhause, V. W. Hughes, R. M. Mobley, R. Prepost, and J. E. Rothberg, *Phys. Rev. Letters* 13, 202 (1964).

²⁹M. Ruderman, *Phys. Rev. Letters* 17, 794 (1966).

³⁰P. A. Thompson, J. J. Amato, P. Crane, V. W. Hughes, R. M. Mobley, G. zu Putlitz, and J. E. Rothberg, *Phys. Rev. Letters* 22, 163 (1969).

³¹G. W. Erickson and D. R. Yennie, *Ann. Phys. (N.Y.)* 35, 271 (1965); 35, 447 (1965); M. F. Soto, Jr., *Phys. Rev. Letters* 17, 1153 (1966).

³²T. Appelquist and S. J. Brodsky, *Phys. Rev. Letters* 24, 562 (1970).

³³F. M. J. Pichanick, R. D. Swift, C. E. Johnson, and V. W. Hughes, *Phys. Rev.* 169, 55 (1968).

³⁴For a discussion of the theory of the helium atom, see C. Schwartz, in *Atomic Physics*, edited by V. W. Hughes, B. Bederson, V. W. Cohen, and F. M. J. Pichanick (Plenum, New York, 1969), p. 71.